Band Excitation in Scanning Probe Microscopy: Recognition and Functional Imaging

S. Jesse,[1] R.K. Vasudevan,[1] L. Collins,[1] E. Strelcov,[1] M.B. Okatan,[1] A. Belianinov,[1] A.P. Baddorf,[1] R. Proksch,[2] and S.V. Kalinin[1]

[1]Center for Nanophase Materials Sciences, Oak Ridge National Laboratory, Oak Ridge, Tennessee 37831; email: sjesse@ornl.gov, sergei2@ornl.gov

[2]Asylum Research, an Oxford Instruments Company, Santa Barbara, California 93117

Annu. Rev. Phys. Chem. 2014. 65:519–36

The *Annual Review of Physical Chemistry* is online at physchem.annualreviews.org

This article's doi: 10.1146/annurev-physchem-040513-103609

Keywords

SPM, ESM, D-PFM

Abstract

Field confinement at the junction between a biased scanning probe microscope's tip and solid surface enables local probing of various bias-induced transformations, such as polarization switching, ionic motion, and electrochemical reactions. The nanoscale size of the biased region, smaller or comparable to that of features such as grain boundaries and dislocations, potentially allows for the study of kinetics and thermodynamics at the level of a single defect. In contrast to classical statistically averaged approaches, this approach allows one to link structure to functionality and deterministically decipher associated mesoscopic and atomistic mechanisms. Furthermore, responses measured as a function of frequency and bias can serve as a fingerprint of local material functionality, allowing for local recognition imaging of inorganic and biological systems. This article reviews current progress in multidimensional scanning probe microscopy techniques based on band excitation time and voltage spectroscopies, including discussions on data acquisition, dimensionality reduction, and visualization, along with future challenges and opportunities for the field.

1. INTRODUCTION

SPM: scanning probe microscopy

AFAM: atomic force acoustic microscopy

PFM: piezoresponse force microscopy

Phase transformations and reactions in solids underpin virtually all aspects of modern science and technology, extending from structural materials to information processing (1) and branching to energy conversion and storage (2–6). It is well recognized that kinetics and thermodynamics of these transitions are controlled by defects that may affect the thermodynamic stability of the phase and serve as nucleation centers for phase transformations and pinning centers for mobile transformation fronts. Defects control the width of transition hysteresis in solid-solid transformations, coercive fields in ferroelectric and ferromagnetic materials, and the overpotential in electrochemical systems and play many other roles. In large concentrations, defects often instigate emergent phenomena such as in ferroelectric relaxors, spin, and cluster glasses (7–9).

Despite the momentous role of defects (and, more generally, microstructure) on virtually all aspects of material functionality, a systematic analysis of the effects presents a considerable challenge. Although the atomic and electronic structure of defects has become accessible because of advances in (scanning) transmission electron microscopy and electron energy loss spectroscopy (10), functionality at the single-defect level remains inaccessible. The consequences of defects are typically analyzed phenomenologically as appropriate spatial and energy distributions are introduced and the dimensionality of transformation process is prescribed, giving rise to Kolmogorov-Avrami-type theories. In comparison, understanding structure-functionality relationships on the single-defect level allows transitions to new levels of predictive modeling and hence the optimization and design of new materials.

The dearth of information about single-defect-level structure-property relationships stems directly from the difficulty of making appropriate measurements. As a relevant parallel example, the development of quantitative molecular unfolding spectroscopy by Rief and colleagues (11) in 1999 provided a robust tool for probing the kinetics and thermodynamics of force-controlled chemical reactions on the single-molecule level, spurring a number of breakthroughs in statistical physics of nanoscale systems. Combined with advances in the synthesis of defined bio- and macromolecules, this led to a revolution in single-molecule biochemistry and recently in photo- and electrochemistry. An obvious challenge for materials science and condensed matter physics is whether this success can be echoed for defect-controlled transformations in solids, including thermal phase transitions in polymers and solids, bias-induced phase transitions in ferroelectrics and antiferroelectrics, and electrochemical processes in energy conversion and storage and electroresistive materials.

2. SCANNING PROBE MICROSCOPIES: FROM STRUCTURE TO FUNCTIONALITY

In the past two decades, scanning probe microscopy (SPM) has emerged as a universal method for probing a material's structure and functionality on the nanoscale. Techniques such as electrostatic and Kelvin probe force microscopy spatially resolve stray electrostatic fields above surfaces; magnetic force microscopy probes near-surface magnetic fields; and atomic force acoustic microscopy (AFAM) and piezoresponse force microscopy (PFM) provide information on local mechanical and electromechanical properties, respectively (15–17).

Probing phase transformations by SPM can include performing measurements in controlled external uniform fields, such as variable temperature studies of magnetic, ferroelectric, superconducting, and structural phase transitions; mechanical and dielectric phenomena in polymers; electrical field polarization switching in ferroelectric capacitors; and mechanical phenomena under strain. In the case of a uniform field, a phase transition is initiated at a small number of nucleation centers and followed by the propagation of transformation fronts through the material. Thus, under a

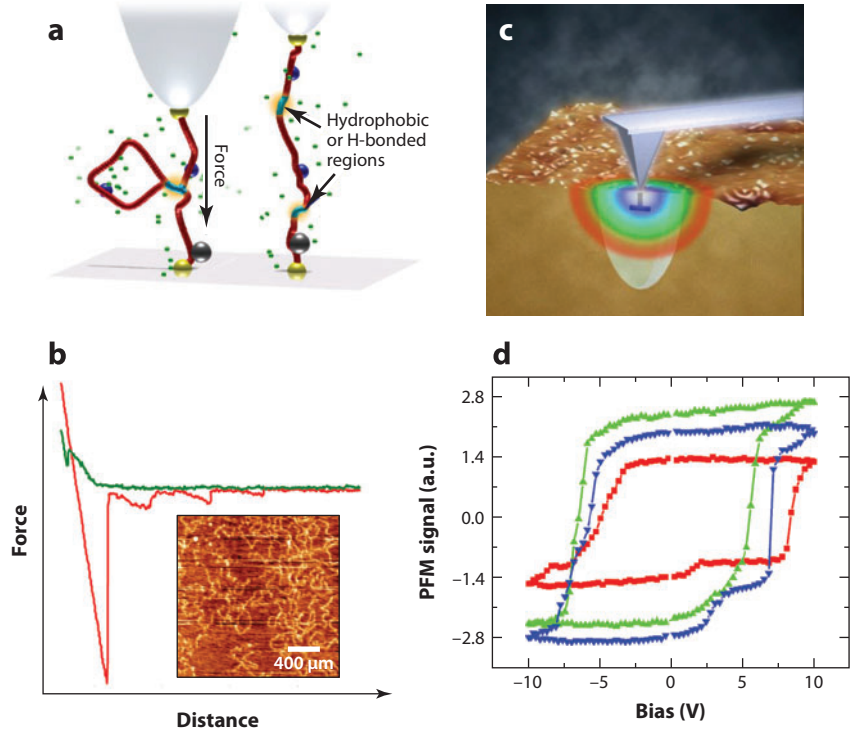

Figure 1

(*a*) Schematic illustration of the unfolding process of a single macromolecule and (*b*) a characteristic force-distance curve. The jumps on the force distance curve correspond to molecular unfolding events, the thermodynamics and kinetics of which can be analyzed. Data in panel *b* courtesy of B. Rodriguez. (*c*) Schematic illustration of a local tip bias-induced phase transformation on the single-defect level as exemplified by polarization switching in a ferroelectric. (*d*) Example of a piezoresponse hysteresis loop fine structure, indicating domain-defect interactions (see 12–14 for details). Panel *d* reprinted with permission from Reference 13. Copyright 2008 by the American Physical Society. Abbreviation: PFM, piezoresponse force microscopy.

uniform field, the transformation is dominated by only a few, widely separated nucleation sites, and even though detection is local, it is not possible to determine the local nucleation properties.

An alternative approach for probing local transformations in solids relies on local SPM-based spectroscopies. In this case, an atomic force microscope tip is used to both induce and detect transformations. That is, the tip concentrates the probing field to a small amount of material (**Figure 1*c***). The field is swept, inducing local transformation, with tip-measured parameters such as current, strain, or microwave response yielding information on local phenomena (**Figure 1*d***). The field confinement approach is complementary to the matter confinement approach traditionally used in nanoscience and offers the advantage of spatially resolved measurements (18, 19). In particular, the location of the probe can be varied along the sample surface, so the response can be probed over a spatial grid (**Figure 2**). For irreversible transitions, the grid is necessarily sparse; in other words, the size of the transformed region must be smaller than the spacing between measurement points. An example includes nanoindentation-based mapping of mechanical properties. At the same time, reversible-transition imaging is possible on a dense grid in which

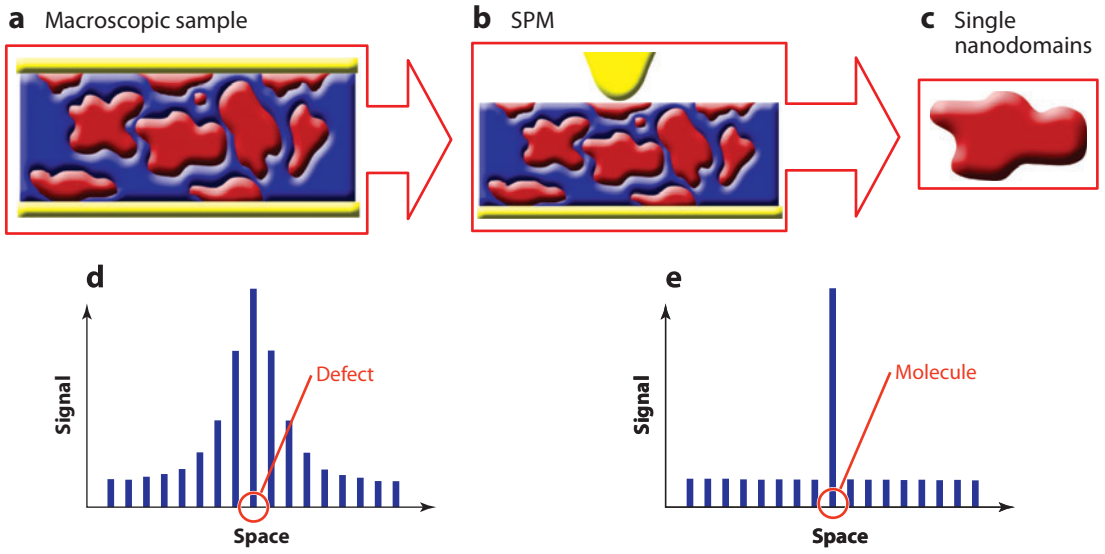

Figure 2

Probing dynamic phenomena in uniform and localized fields. In macroscopic measurements (*a*), the collective response of all structural elements is probed. In the scanning probe microscopy (SPM) case (*b*), the response is localized. However, for uniform fields, all parts of the sample are excited, whereas for local fields, the long-range electrostatic and strain interactions preclude the response of an individual structural element to be defined. At the same time, unlike the case for a molecule, a single microstructural element (*c*) cannot be isolated outside the lattice. This behavior imposes stringent requirements on the acquisition and analysis of SPM data: Spatially resolved spectroscopic imaging is required to probe single-defect functionality in solids (*d*), whereas single-point spectroscopic measurements are required for molecular unfolding spectroscopy (*e*) (i.e., responses from adjacent spatial locations are uncorrelated).

probing volumes can be larger than the pixel spacing. This presents a pathway for high–spatial resolution studies. Examples include electric field–induced ferroelectric switching (20), some electrochemical processes (21), and temperature-induced reversible transformations (22).

Spectroscopic probing of local transformations necessarily brings forward the challenge of quantitative SPM measurements. Whereas imaging in the external field relies on qualitative contrast from which, for example, a ferroic domain structure or phase distribution can be deduced, spectroscopic imaging requires the relationship between the measured signal and the degree of transformation to be known. As such, one must ascertain the relationship among the local response, undetermined probe parameters, and the microscope transfer function. The first factor can be readily illustrated by topographic cross talk (i.e., the possible interdependence between the measured SPM signal and local surface topography). In particular, mechanical parameters such as contact stiffness and work of adhesion scale linearly with the tip-surface contact area. Correspondingly, for an otherwise homogeneous material, protrusions on the surface are always effectively softer and depressions are always harder. This topographic cross talk follows from the classical indentation mechanics and intrinsic material properties (e.g., Young's modulus) for which topographic effects cannot be unambiguously separated from local measurements alone. As an example, in molecular unfolding spectroscopy, the force exerted by an SPM probe can be readily calibrated, and the geometrical size of the system (i.e., molecular cross section) is well known and constant throughout the measurement. In contrast, for indentation measurements, the tip-surface contact is a priori unknown, and it changes during the measurement. Correspondingly, quantification is highly nontrivial and is possible only for a carefully analyzed indentor shape, in combination with, for example, the use of the Oliver-Pharr method (23).

In comparison, the classical electromechanical response of the tip-surface junction for piezoelectric materials is independent of the tip-surface contact radius (24, 25). Therefore, electromechanical imaging is intrinsically quantitative, and small changes in the signal responding to the electric field can be interpreted as a change of material properties below the tip, rather than changes in contact area. The same is true for an electrochemical strain signal for a diffusion-coupled process, albeit not necessarily for all electrochemical strain-generation mechanisms. Finally, the tip-surface contact area can be fixed (although unknown) using a freeze-in approach recently proposed for thermal SPM measurements (22), analogous to the Oliver-Pharr method.

BE: band excitation

Another requirement is the quantitative knowledge of the microscope transfer function that defines the relationship between the local signal generated at the tip-surface junction and the external data-storage system. Many contributions to the microscope transfer function, such as photodiode sensitivity and amplifier characteristics, are independent of the material and can be calibrated or assumed constant during the measurement (26). However, parameters such as the resonant frequency of the tip-surface junction are dependent of the surface topography, potentially leading to indirect topographic cross talk (27).

Specific to techniques based on the detection of cantilever motion, quantitative measurements require information on the local cantilever transfer function (e.g., amplitude and phase versus the frequency response of the probe). In an idealized system, at low frequencies, the amplitude is constant, and the frequency dispersion becomes significant as the first resonant frequency is approached. Practically, even a low-frequency response is affected by a nonideal transfer function (28). More importantly, consideration of resonance enhancement in weak surface responses compels one to probe the segment of the response curve containing the resonance; techniques include band excitation (BE) SPM (29, 30), fast frequency scans (31), rapid imaging (32), and ring-down methods (33). In special cases, similar information can sometimes be obtained using amplitude-based resonance tracing or cantilevers with built-in amplifiers.

3. FREQUENCY 3D SCANNING PROBE MICROSCOPY: BAND EXCITATION

In BE, the system is excited by a digitally synthesized signal having a finite spectral density in a band centered on a resonance peak (29, 34), as shown in **Figure 3**. This signal substitutes the single sine wave used in classical SPM (which corresponds to a delta function in Fourier space). The response is detected in the usual fashion (e.g., using a photodetector) and is Fourier transformed. The ratio of the fast Fourier transforms of the response and excitation signals yields the transfer function of the system. The resulting frequency dependence of the response can be analyzed to yield parameters of the oscillator, including the amplitude, resonant frequency, and Q factor.

The implementation of BE methods requires an interpretation of the three-dimensional (3D) $A(x, y, \omega)$ and $\theta(x, y, \omega)$ data arrays, where $\{A, \theta\}$ is the response amplitude and phase and ω is the frequency. Ideally, interpretation of the data includes (*a*) dimensionality reduction and (*b*) parameter extraction. Dimensionality reduction includes the reduction of the 3D, or higher dimensional, data set into 2D spatially resolved maps that are easier to interpret. This transformation can be based on the physical meaning of the data or on statistical projection techniques.

In PFM, for contact resonances with small damping, one can describe the amplitude-frequency response of the cantilever in contact with the surface using the simple harmonic oscillator model (35):

$$H(\omega) = \frac{A_i^{\max}\omega_{i0}^2 e^{i\varphi}}{\omega^2 - i\frac{\omega\omega_{i0}}{Q_i} - \omega_{i0}^2}, \quad (1)$$

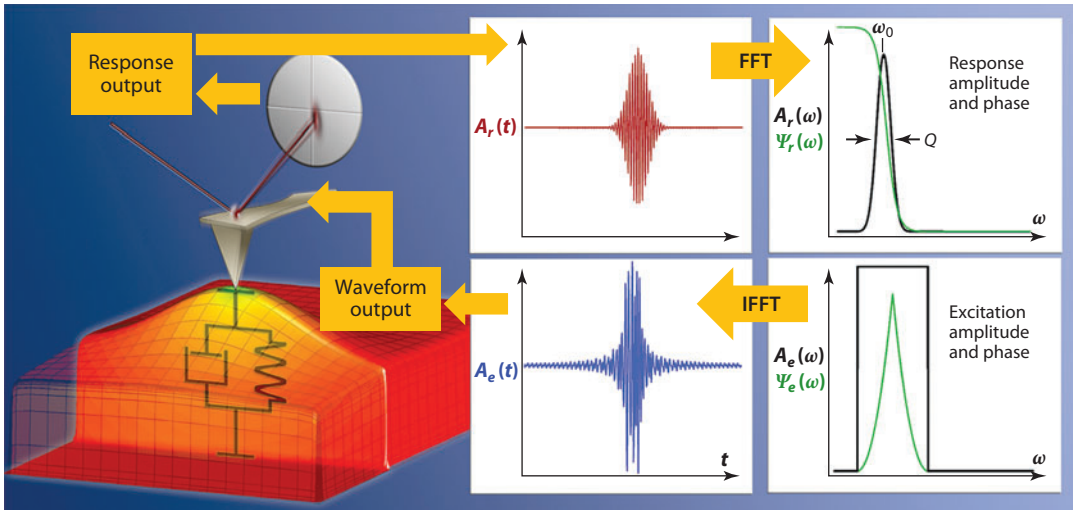

Figure 3

Schematic illustration of the band excitation method. The signal with predefined amplitude and phase content is defined in the Fourier domain and inverse Fourier transformed to the time domain. Thus the obtained signal is used as an excitation in scanning probe microscopy, substituting classical sinusoidal excitation. The detected response is Fourier transformed, and the ratio of the response and excitation signals yields the local band excitation response of the system. Figure reprinted from Reference 29, © IOP Publishing. Reproduced by permission of IOP Publishing. All rights reserved. Abbreviations: FFT, fast Fourier transform; IFFT, inverse fast Fourier transform.

where $A_i^{\max}$ is the amplitude signal at the frequency of i-th resonance, ω_{i0}, and Q_i is the quality factor that describes energy losses in the system. Using this approach, one can fit the 3D data to the simple harmonic oscillator model to extract and plot 2D maps of its parameters: the response amplitude, resonance frequency, and Q factor.

BE spectroscopies can be further extended to explore a family of different transitions induced by the confined field at the tip-surface junction. All first-order phase transitions are hysteretic and hence history dependent. This necessitates first-order reversal-curve-type studies, effectively increasing the dimensionality of the data (**Figure 4*a*,*b***) (36). Furthermore, first-order phase transitions often possess slow time dynamics, making it necessary to probe kinetic hysteresis (and differentiating it from thermodynamics) by measuring the response as a function of time. Finally, the detection of force-based SPM requires one to probe the response in a frequency band around the resonance (as the resonant frequency can be dependent on position, and single-frequency methods fail to capture these changes). These simple physical arguments illustrate that the complete probing of local transformations requires a 6D [space × frequency × (stimulus × stimulus) × time] detection scheme. **Table 1** and **Figure 4*c*** illustrate the development of these techniques.

The BE method can be broadly applied to any contact resonance-based atomic force microscopy (AFM). In addition to PFM, these include ultrasonic force microscopy (75) and AFAM (76) used for mapping nanomechanical properties. In the following sections, we take a closer look at some AFM techniques employing BE modes.

AFM: atomic force microscopy

4. DYNAMIC ATOMIC FORCE ACOUSTIC MICROSCOPY

In AFAM, the sample is mechanically excited using an ultrasonic transducer causing an out-of-plane surface displacement (76). This further excites flexural vibration modes of the cantilever

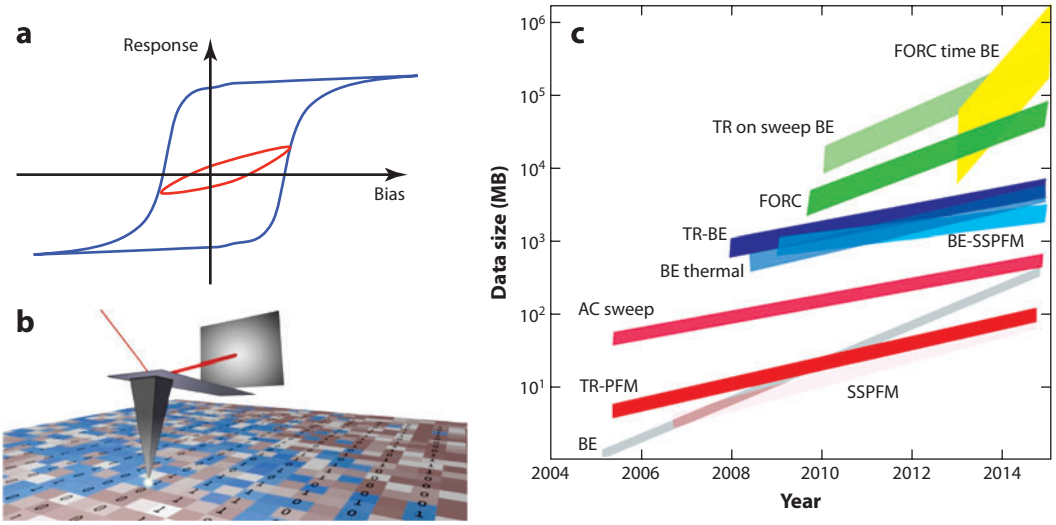

Figure 4

(*a*) Schematic illustration of the hysteretic responses including the minor hysteresis loop, showing the necessity of the first-order reversal-curve measurements to explore the field history dependence of responses across (*b*) the sample surface. (*c*) Evolution of the information volume in multidimensional scanning probe microscopies (see **Table 1**). Abbreviations: AC, alternating current; BE, band excitation; FORC, first-order reversal curve; PFM, piezoresponse force microscopy; SSPFM, switching spectroscopy piezoresponse force microscopy; TR, time relaxation.

(**Figure 5*a***). Operating close to cantilever vibrational modes allows for improved signal-to-noise ratios through resonant amplification, and the technique is often referred to as contact-resonance atomic force microscopy (CR-AFM) (77, 78). Many different approaches have been implemented to obtain information on the mechanical properties of the sample using CR-AFM.

Historically, spatial variation in mechanical properties is obtained using single-frequency excitation, with the excitation signal close to the cantilever contact resonance; lock-in techniques

Table 1 Development of multidimensional scanning probe microscopy methods at Oak Ridge National Laboratory

Technique	Dimensionality	Current data set	References
BE	3D; space and ω	(256 × 256) × 64	29, 33, 37–40
SSPFM	3D; space and voltage	(64 × 64) × 128	14, 20, 41–49
Time relaxation PFM	3D; space and time	(64 × 64) × 128	50–52
AC sweeps	4D; space, ω, and voltage	(64 × 64) × 64 × 256	53, 54
BE SSPFM	4D; space, ω, and voltage	(64 × 64) × 64 × 128	55–61
BE thermal	4D; space, ω, and temperature	(64 × 64) × 64 × 256	22, 62–64
Time relaxation BE	4D; space, ω, and time	(64 × 64) × 64 × 64	65–67
First-order reversal curves	5D; space, ω, voltage, and number of sweeps	(64 × 64) × 64 × 64 × 16	68–72
Time relaxation on sweep, BE	5D; space, ω, voltage, and time	(64 × 64) × 64 × 64 × 64	73, 74
FORC time BE	6D; space, ω, voltage, number of sweeps, and time	(64 × 64) × 64 × 64 × 16 × 64	Not yet realized

Abbreviations: AC, alternating current; BE, band excitation; FORC, first-order reversal curve; PFM, piezoresponse force microscopy; SSPFM, switching spectroscopy piezoresponse force microscopy.

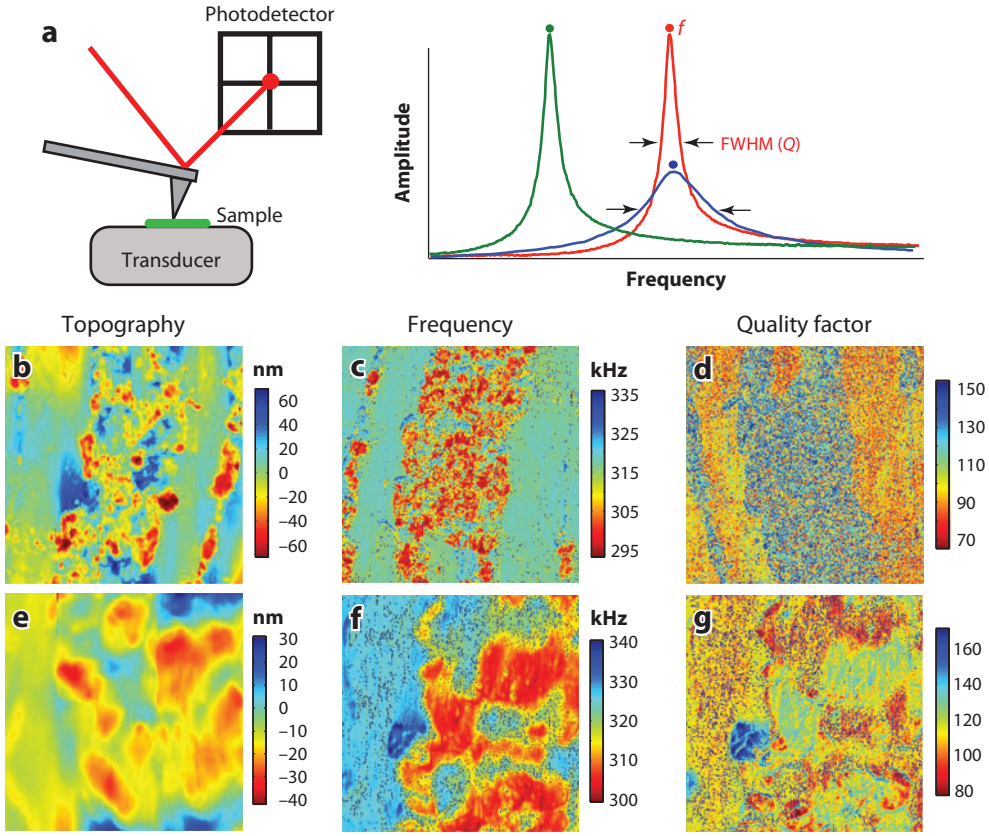

Figure 5

(*a*) Principle of contact-resonance atomic force acoustic microscopy. The tip-to-sample contact is excited by mounting a sample on a transducer that excites flexural modes in the cantilever. The contact-resonance frequency and quality factor, *Q*, will shift with changes in the elastic modulus and viscous properties of the sample, respectively. Shown are the (*b*,*e*) topography, (*c*,*f*) frequency maps, and (*d*,*g*) quality factor maps of the viscoelastic variation on a polished coal surface collected using band excitation atomic force acoustic microscopy. Abbreviation: FWHM, full width at half maximum.

are then used to detect changes in the amplitude response. These changes are shifts in either the contact-resonance frequency's conservative forces or the *Q* factor's dissipative processes and have been used to infer qualitative changes in mechanical properties of the sample (77). Interpretation of amplitude data in this way, however, is challenging, especially for complex heterogeneous samples, and it is extremely dependent on the frequency (79). Despite these challenges, CR-AFM techniques capable of mapping changes in the contact-resonance frequency have proven useful for studying the contact stiffness and elastic modulus through changes in the conservative forces acting on the cantilever (80, 81). This approach usually involves point-contact resonance spectroscopy in which the full frequency spectrum is obtained at each pixel by chirping the excitation signal. However, such an approach can be time-consuming and presents a trade-off between the spatial resolution and acquisition time (82–84), although improvements in image-acquisition times have recently been achieved (85, 86). Furthermore, on compliant materials, it is necessary to determine both elastic and viscous material properties, which requires the decoupling of conservative and dissipation tip-sample interactions. Single-frequency CR-AFM techniques lack the ability to separate the contributions from these properties.

Therefore, CR-AFM measurements must be extended beyond single-frequency techniques and must track not only changes in the resonant frequency but also the Q factor of the AFM cantilever to determine both conservative and dissipative material properties (87). In this case, multifrequency techniques such as BE or dual-frequency resonance tracking are required to map both the elasticity and dissipation (88) and have been used for quantitative viscoelastic mapping of polymer blends (88, 89). The increased amount of information obtained in such a multidimensional approach provides insight into the tip-sample forces that is unavailable in single-frequency AFAM measurements.

CR-AFM: contact-resonance atomic force microscopy

ESM: electrochemical strain microscopy

Figure 5 shows BE-AFAM data collected on a polished coal sample, collected from an underground mine in the subbituminous/bituminous region of the Uintah Basin located in Colorado. The coal structure on the submillimeter level is highly inhomogeneous, and a set of compound elements (lithotypes, microlithotypes, and macerals) can be defined (90, 91). The structure and nanomechanical properties of individual macerals remain largely unknown, despite their importance for understanding and improving mining and utilization (e.g., coke formation) approaches and techniques (92). The BE-AFAM data clearly show that coal consists of regions with different elastic moduli and dissipation or loss moduli corresponding to changes in the resonant frequency and Q values, respectively. We note the complex internal structure of the coal sample revealed by AFAM imaging.

5. DYNAMIC ELECTROCHEMICAL STRAIN MICROSCOPY

The voltage response of many ferroic systems is strongly dependent on bias sweep rates, suggesting that the kinetics of the transformation process can be an important factor (7). Upon excitation (e.g., bias), the temporal dynamics of the response provides insight on the stability of the formed phase and its aging, revealing interactions between the newly made domain and domain walls with intrinsic disorder. Furthermore, multiple other mechanisms can give rise to relaxational dynamics, with examples ranging from surface charge screening in polar materials (93), to more complex transitions in relaxor ferroelectrics (94), to vacancy and ionic motion in ionic conductors (65, 95). Therefore, complete characterization requires the probing of the system response as a function of the external excitation and the time after the excitation is removed. This characteristic timescale can span the range from nanoseconds to several minutes, or even hours, requiring systematic studies of the response over multiple decades. Accordingly, the system response can then (possibly) be decoupled into its constituent thermodynamic and kinetic parts.

To visualize and explore these voltage- and time-dependent dynamic behaviors, researchers have introduced dynamic PFM (73, 96) and dynamic electrochemical strain microscopy (ESM). In these techniques, a stepped triangular direct current (DC) waveform is applied to the tip to investigate hysteretic phenomena (**Figure 6*a***). The BE response is registered after each pulse for a period of ~1–30 s, which can be adjusted as required. **Figure 6*b*** shows a typical BE (ESM) response for a single point. The high amplitude of the response is apparent for the positive part of the bias, whereas a lower amplitude is found for the negative bias. Additionally, relaxation after each bias pulse is also clearly evident. Fitting with a suitable function, one can reduce the amplitude of the ESM response to a function of $V(x, t)$, which is plotted in **Figure 6*c***. The response after each DC pulse shows relaxation, with the highest relaxation found for large positive or negative bias, and minimal relaxation found for smaller DC pulses.

These point spectroscopies can be performed over a grid of points to allow for the mapping of spatial correlations in the relaxation behavior. To visualize the multidimensional data sets and correlate voltage-dependent dynamic behavior to microstructure, one must first reduce the data dimensionality. This goal may be achieved by fitting a function (providing that suitable

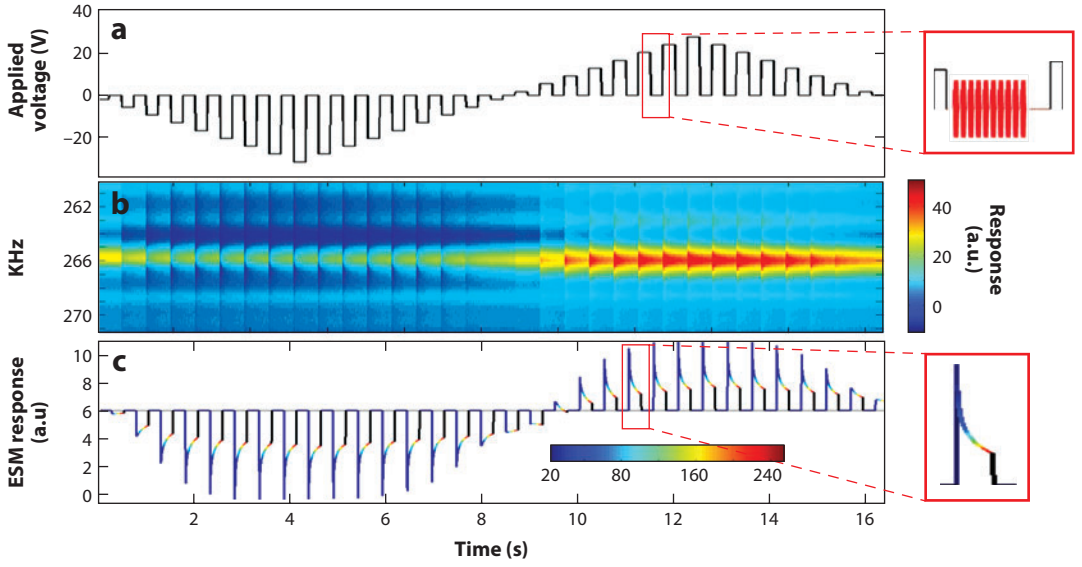

Figure 6

Point spectroscopy in dynamic electrochemical strain microscopy (ESM) mode. (*a*) A DC train of pulses is applied to the scanning probe microscope tip, with the response probed by band excitation waveforms as a function of time after each pulse (*inset*). (*b*) The captured ESM response clearly shows a larger response for positive bias and a lower response for negative bias. The relaxation after each pulse is also evident. (*c*) Fitting the data to a simple harmonic oscillator function allows the response amplitude to be plotted. The relaxation appears greater for larger bias but is small for lower voltages. Figure adapted with permission from Reference 74. Copyright Nature Publishing Group.

physics-based analytical models exist); phenomenological fitting; or more robust, but difficult to interpret, quantitative statistical methods such as principal component analysis (PCA). Regardless, spatial mapping of the parameters describing the relaxation behavior allows the correlation to the microstructural features of the sample, which can provide information on local physics and chemistry.

An example of dynamic ESM (**Figure 7*a***) is a topography image of yttria-stabilized zirconia (74). In this material, applying a bias to the tip can activate oxygen evolution and reduction reactions at the tip-surface junction. This changes the local oxygen vacancy concentration and the measured ESM signal. After the bias pulse, a slow diffusion takes place that is kinetically controlled by the motion of the vacancies (or other ionic species), causing relaxation of the ESM signal over time. The reactivity of the yttria-stabilized zirconia surface, defined as the area under the ESM loop, is clearly spatially dependent (**Figure 7*b*,*c***). An ESM loop is captured at a single point as a function of time (from 0 to 250 ms) (**Figure 7*d***). It is immediately evident from **Figure 7*a*** that the loop relaxes significantly, moving from an elongated shape to a more straight-edged loop over a period of just a few milliseconds. Fitting the ESM signal to an exponential decay model, $R(V, t) = R_0(V) + R_1(V)\exp[-t/t(V)]$, allows the static, i.e., nonrelaxing, term $R_0(V)$ and the relaxing amplitude $R_1(V)$ to be plotted as a function of bias (**Figure 7*b*,*c***). The static portion is clearly hysteretic with bias, whereas the relaxing amplitude varies sigmoidally, suggesting that the thermodynamic and kinetic components can indeed be separated. For small bias values, the relaxation is relatively linear; however, at a higher bias, there is a saturation, indicating the stability of the system (i.e., small relaxations) for small perturbations. These studies highlight both the utility and necessity of dynamic ESM in determining kinetic and thermodynamic contributions to the system response.

PCA: principal component analysis

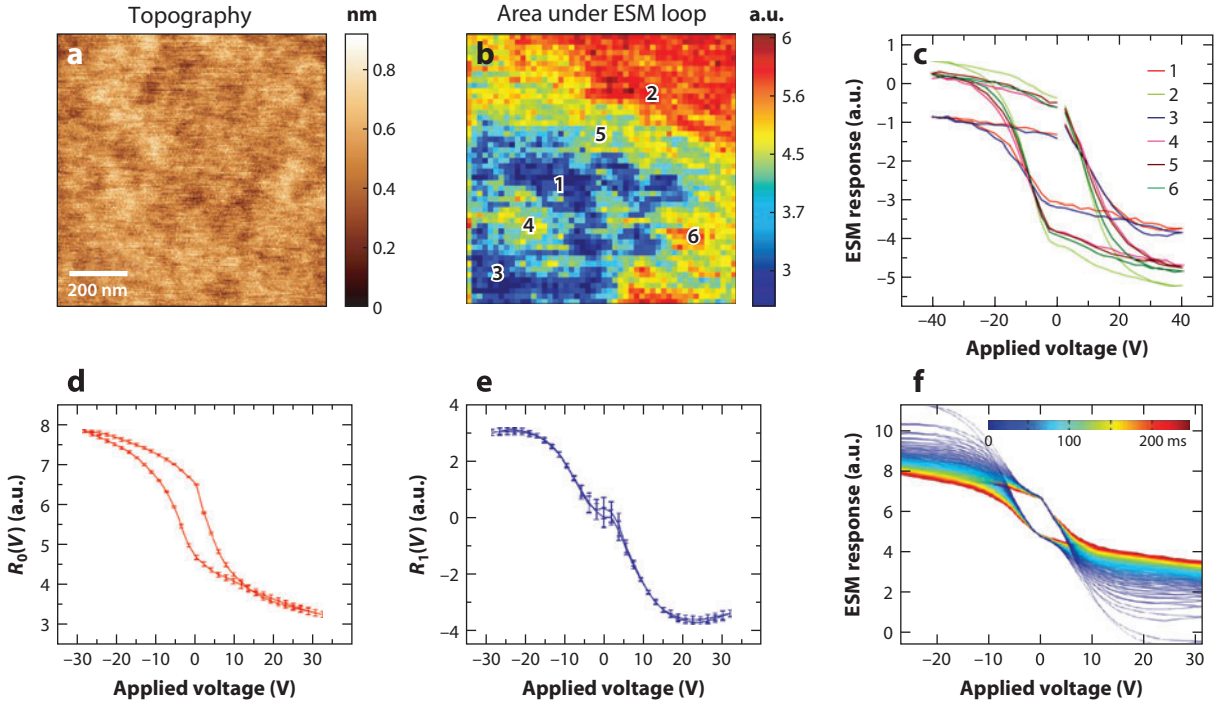

Figure 7

Dynamic electrochemical strain microscopy (ESM) spectroscopy to separate thermodynamics from kinetics. (*a*) The topography and (*b*) a reactivity map of the surface of yttria-stabilized zirconia, defined as the area under the ESM loop. (*c*) Selected loops from panel *b*. Dynamic ESM is then performed to separate the thermodynamic and kinetic components. Functional fits allow extraction of the (*d*) time-independent and (*e*) time-dependent terms of the relaxation response to be captured. (*f*) A selected loop and its variation over 300 ms. Figure reprinted with permission from Reference 74. Copyright Nature Publishing Group.

6. RECOGNITION IMAGING BASED ON FREQUENCY-DEPENDENT ELECTROMECHANICAL RESPONSE

An alternative approach to data analysis in BE is based on the purely statistical variations of the frequency-dependent responses using statistical projection techniques such as PCA, independent component analysis, and factor analysis (97, p. 936). This approach allows one to image functional structures using recognition of the local functionality, in which the local frequency response acts as a fingerprint. This recognition is effectively associative thinking modeled after a human brain, with the additional advantage of the numerical precision and error estimation of a mathematical model. Furthermore, this approach obviates the need for a physical model of observed responses (except for obvious microscope calibration) by directly linking the response to target functionalities. The operation of functional recognition SPM (39) includes the steps of training a neural net using a set of examples, data acquisition, and feature recognition (**Figure 8**).

At the training stage, the neural network is configured to recognize material functionality for a set of training examples provided by the observer. PCA is used on the structure of the resulting 3D, or higher dimensional, data set to simplify and decorrelate the data. Thus predetermined parameter vectors are employed to train a feedforward neural network using PCA loadings as an input and parameters describing the material functionality as a target.

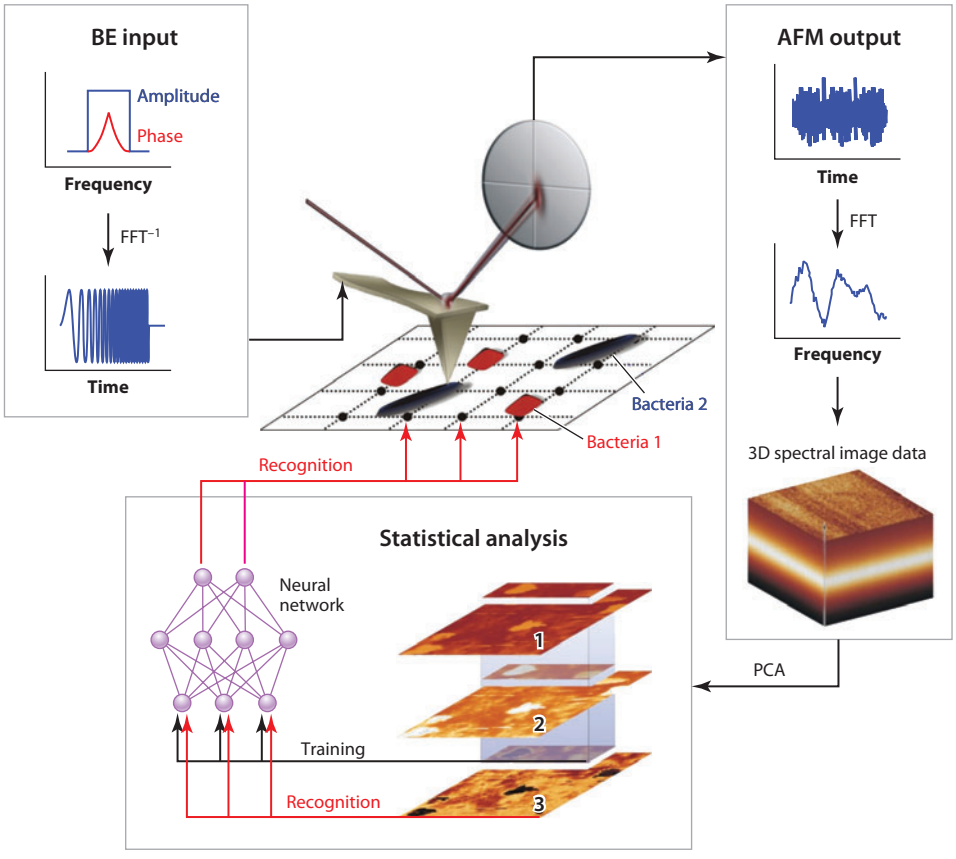

Figure 8

Recognition band excitation (BE) imaging. The 3D spectroscopic BE array is decorrelated using principal component analysis (PCA). The subset of the image with known functionality is used as a training example for the neural net. Thus the trained neural net is used to recognize the remaining part of the image. A similar approach can be employed for a neural net trained using external examples. Abbreviations: AFM, atomic force microscopy; FFT, fast Fourier transform.

In the recognition stage, one analyzes the measured SPM signal using a pretrained neural network to provide a map of the material functionality. The measured response is projected onto the PCA eigenvectors, with the deconvoluted components of multispectral data, at each pixel, acting as inputs for the previously trained neural network. The network output yields material property maps. The main advantage of such an approach is that the decorrelation and neural network processing are linear and algebraic operations, which imply that data processing is fast. Reciprocally, the flexibility of neural network algorithms precludes the need for human supervision during analysis of multiple spectra once a target set is established. Finally, the recognition error of the neural net can be used as an indicator of the responses absent in the original training set.

Figure 9 illustrates functional recognition SPM for PFM-based electromechanical imaging of bacteria in a liquid environment. As a model system, *Micrococcus lysodeikticus* and *Pseudomonas fluorescens* bacteria are deposited on the poly-lysine-coated mica. The two can be identified based

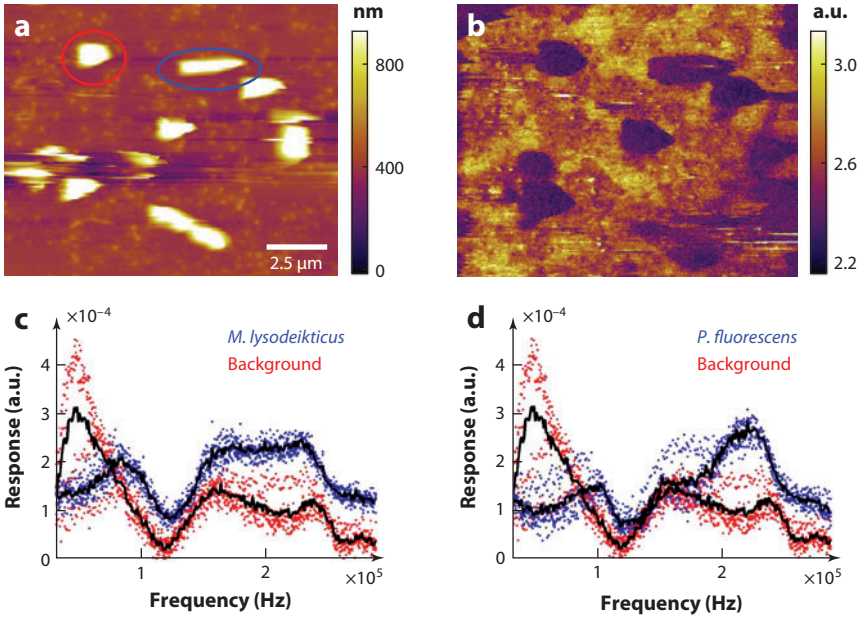

Figure 9

Recognition imaging. (*a*) Surface topography of *Micrococcus lysodeikticus* and *Pseudomonas fluorescens* bacteria. Two bacteria (*red and blue ellipses*) can be identified based on the characteristic shape. (*b*) Single-frequency piezoresponse force microscopy amplitude image recorded in liquid. (*c*,*d*) Comparison of the frequency-dependent response for different bacteria types versus substrate, illustrating complex but distinct frequency responses. Panel *a* reprinted from Reference 39, © IOP Publishing. Reproduced by permission of IOP Publishing. All rights reserved.

on the characteristic shape in the topographic image of bacteria; however, the nature of other surface features is uncertain. Their origin can include bacterial fragments or contaminates.

The single-frequency PFM image in **Figure 9*b*** illustrates the presence of a strong electromechanical response on bacterial systems. However, no systematic difference between the two bacteria can be observed at any given frequency. At the same time, BE PFM allows one to collect information in the broad frequency range. The amplitude frequency response curves averaged over regions with known identity (two bacteria types and substrate) illustrate a significant difference between the spectral responses of the bacteria and substrate.

While the signal variability at any single frequency is too large and insufficient for unambigous identification, the recognition analysis of spectral data as shown in **Figure 8** allows one to overcome this problem. The amplitude-frequency response curves are decorrelated using PCA. The resulting loadings taken from the selected subset of the image with readily identifiable bacterial and substrate regions are used to train the neural network using the loadings as an input and bacterial type as an output. Thus the trained network is used on the whole image to identify the rest of the objects in it. **Figure 10** shows the outputs on the channels corresponding to individual types and the identification image. We note the near-perfect identification of the bacteria in the remainder of the image, readily verifiable based on shape. Some topographic features are not identified as bacteria, suggesting that these can be extraneous particles. At the same time, a segment of the surface is identified as *M. lysodeikticus*, suggesting the potential presence of a flat cellular membrane.

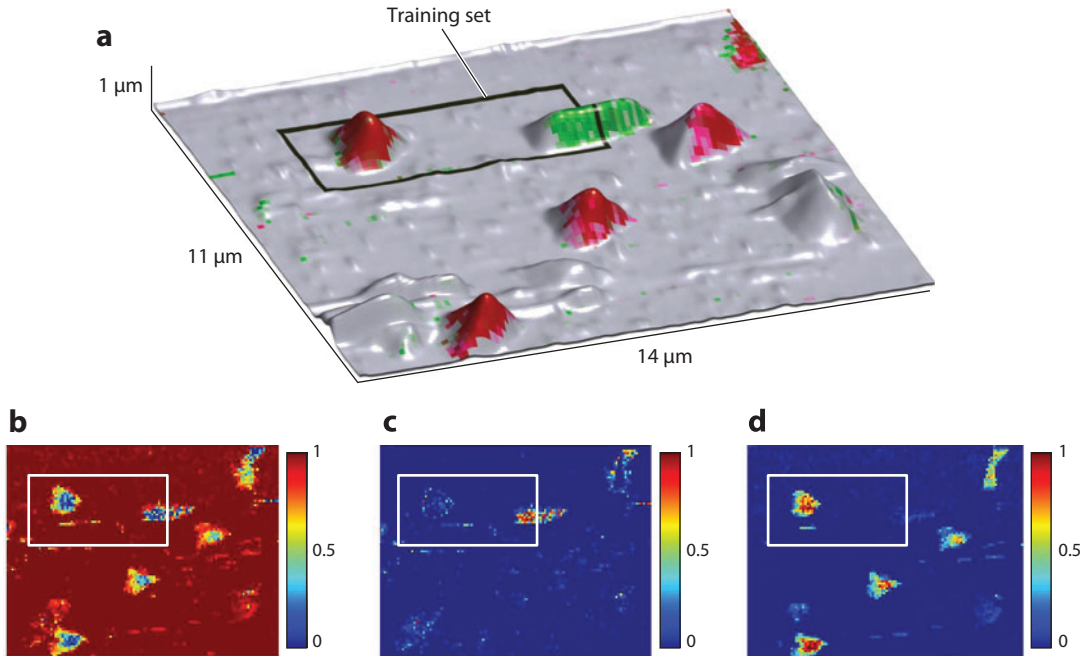

Figure 10

(*a*) Recognition imaging of individual bacterial responses overlaid on the topographic image and individual maps corresponding to the (*b*) background, (*c*) *Pseudomonas fluorescens* response, and (*d*) *Micrococcus lysodeikticus* response. Figure reprinted from Reference 39, © IOP Publishing. Reproduced by permission of IOP Publishing. All rights reserved.

7. SUMMARY

Electric and thermal field confinement at the tip-surface junction in SPM allows systematic studies of field-induced phase transitions and reversible and irreversible electrochemical reactions. However, the hysteretic nature and often-present slow time dynamics necessitate the development of complex multidimensional time- and voltage-dependent spectroscopies to capture relevant aspects of system behaviors. Furthermore, quantitative measurements of associated responses require compensation for the tip-surface transfer function. This goal is achieved through the BE method, enabled by the parallel probing response in the frequency band containing the cantilever resonance. This approach allows both quantitative probing of material functionality for known physical models of the response and recognition imaging based on predefined responses. Although the present review focuses predominantly on electromechanical SPM techniques, the same approach can be used for a broad range of mechanical, magnetic, and electric imaging.

DISCLOSURE STATEMENT

S.J. and S.V.K. hold a licensed patent for the BE method described herein, for which they receive royalties. R.P. is an employee of Asylum Research, an Oxford Instruments company, a manufacturer of atomic force microscopes.

ACKNOWLEDGMENTS

This research was conducted at the Center for Nanophase Materials Sciences, which is sponsored at the Oak Ridge National Laboratory by the Scientific User Facilities Division, Office of Basic Energy Sciences, US Department of Energy.

LITERATURE CITED

1. Waser R. 2012. *Nanoelectronics and Information Technology*. Weinheim, Ger.: Wiley-VCH
2. Bagotsky VS. 2009. *Fuel Cells: Problems and Solutions*. New York: Wiley
3. Tarascon JM, Armand M. 2001. Issues and challenges facing rechargeable lithium batteries. *Nature* 414:359–67
4. Kraytsberg A, Ein-Eli Y. 2011. Review on Li-air batteries: opportunities, limitations and perspective. *J. Power Sources* 196:886–93
5. Girishkumar G, McCloskey B, Luntz AC, Swanson S, Wilcke W. 2010. Lithium-air battery: promise and challenges. *J. Phys. Chem. Lett.* 1:2193–203
6. Ormerod RM. 2003. Solid oxide fuel cells. *Chem. Soc. Rev.* 32:17–28
7. Tagantsev AK, Cross LE, Fousek J. 2010. *Domains in Ferroic Crystals and Thin Films*. New York: Springer
8. Binder K, Young AP. 1986. Spin glasses: experimental facts, theoretical concepts, and open questions. *Rev. Mod. Phys.* 58:801–976
9. Binder K, Reger JD. 1992. Theory of orientational glasses: models, concepts, simulations. *Adv. Phys.* 41:547–627
10. Pennycook SJ, Varela M, Lupini AR, Oxley MP, Chisholm MF. 2009. Atomic-resolution spectroscopic imaging: past, present and future. *J. Electron Microsc.* 58:87–97
11. Rief M, Pascual J, Saraste M, Gaub HE. 1999. Single molecule force spectroscopy of spectrin repeats: low unfolding forces in helix bundles. *J. Mol. Biol.* 286:553–61
12. Morozovska AN, Svechnikov SV, Eliseev EA, Rodriguez BJ, Jesse S, Kalinin SV. 2008. Local polarization switching in the presence of surface-charged defects: microscopic mechanisms and piezoresponse force spectroscopy observations. *Phys. Rev. B* 78:054101
13. Kalinin SV, Jesse S, Rodriguez BJ, Chu YH, Ramesh R, et al. 2008. Probing the role of single defects on the thermodynamics of electric-field induced phase transitions. *Phys. Rev. Lett.* 100:155703
14. Rodriguez BJ, Choudhury S, Chu YH, Bhattacharyya A, Jesse S, et al. 2009. Unraveling deterministic mesoscopic polarization switching mechanisms: spatially resolved studies of a tilt grain boundary in bismuth ferrite. *Adv. Funct. Mater.* 19:2053–63
15. Kalinin SV, Shao R, Bonnell DA. 2005. Local phenomena in oxides by advanced scanning probe microscopy. *J. Am. Ceram. Soc.* 88:1077–98
16. Gerber C, Lang HP. 2006. How the doors to the nanoworld were opened. *Nat. Nanotechnol.* 1:3–5
17. Sadewasser S, Glatzel T, eds. 2011. *Kelvin Probe Force Microscopy: Measuring and Compensating Electrostatic Forces*. New York: Springer
18. Kalinin SV, Rodriguez BJ, Jesse S, Maksymovych P, Seal K, et al. 2008. Local bias-induced phase transitions. *Mater. Today* 11:16–27
19. Kalinin SV, Rodriguez BJ, Jesse S, Chu YH, Zhao T, et al. 2007. Intrinsic single-domain switching in ferroelectric materials on a nearly ideal surface. *Proc. Natl. Acad. Sci. USA* 104:20204–9
20. Jesse S, Lee HN, Kalinin SV. 2006. Quantitative mapping of switching behavior in piezoresponse force microscopy. *Rev. Sci. Instrum.* 77:073702
21. Balke N, Jesse S, Morozovska AN, Eliseev E, Chung DW, et al. 2010. Nanoscale mapping of ion diffusion in a lithium-ion battery cathode. *Nat. Nanotechnol.* 5:749–54
22. Jesse S, Nikiforov MP, Germinario LT, Kalinin SV. 2008. Local thermomechanical characterization of phase transitions using band excitation atomic force acoustic microscopy with heated probe. *Appl. Phys. Lett.* 93:073104
23. Oliver WC, Pharr GM. 1992. An improved technique for determining hardness and elastic modulus using load and displacement sensing indentation experiments. *J. Mater. Res.* 7:1564–83

24. Kalinin SV, Karapetian E, Kachanov M. 2004. Nanoelectromechanics of piezoresponse force microscopy. *Phys. Rev. B* 70:184101
25. Karapetian E, Kachanov M, Kalinin SV. 2005. Nanoelectromechanics of piezoelectric indentation and applications to scanning probe microscopies of ferroelectric materials. *Philos. Mag.* 85:1017–51
26. Butt HJ, Cappella B, Kappl M. 2005. Force measurements with the atomic force microscope: technique, interpretation and applications. *Surf. Sci. Rep.* 59:1–152
27. Jesse S, Guo S, Kumar A, Rodriguez BJ, Proksch R, Kalinin SV. 2010. Resolution theory, and static and frequency-dependent cross-talk in piezoresponse force microscopy. *Nanotechnology* 21:405703
28. Soergel E. 2011. Piezoresponse force microscopy (PFM). *J. Phys. D* 44:464003
29. Jesse S, Kalinin SV, Proksch R, Baddorf AP, Rodriguez BJ. 2007. The band excitation method in scanning probe microscopy for rapid mapping of energy dissipation on the nanoscale. *Nanotechnology* 18:435503
30. Jesse S, Kalinin SV. 2011. Band excitation in scanning probe microscopy: sines of change. *J. Phys. D* 44:464006
31. Kos AB, Hurley DC. 2008. Nanomechanical mapping with resonance tracking scanned probe microscope. *Meas. Sci. Technol.* 19:015504
32. Nath R, Chu YH, Polomoff NA, Ramesh R, Huey BD. 2008. High speed piezoresponse force microscopy: <1 frame per second nanoscale imaging. *Appl. Phys. Lett.* 93:072905
33. Kalinin SV, Jesse S, Proksch R. 2008. Information acquisition & processing in scanning probe microscopy. *R&D Mag.* 50(4):20
34. Kalinin SV, Rodriguez BJ, Jesse S, Proksch R. 2007. A biased view of the nanoworld: electromechanical imaging. *R&D Mag.* 49:34–36
35. Garcia R, Perez R. 2002. Dynamic atomic force microscopy methods. *Surf. Sci. Rep.* 47:197–301
36. Mayergoyz ID, Friedman G. 1988. Generalized Preisach model of hysteresis. *IEEE Trans. Magn.* 24:212–17
37. Jesse S, Mirman B, Kalinin SV. 2006. Resonance enhancement in piezoresponse force microscopy: mapping electromechanical activity, contact stiffness, and *Q* factor. *Appl. Phys. Lett.* 89:022906
38. Jesse S, Kalinin SV. 2009. Principal component and spatial correlation analysis of spectroscopic-imaging data in scanning probe microscopy. *Nanotechnology* 20:085714
39. Nikiforov MP, Reukov VV, Thompson GL, Vertegel AA, Guo S, et al. 2009. Functional recognition imaging using artificial neural networks: applications to rapid cellular identification via broadband electromechanical response. *Nanotechnology* 20:405708
40. Nikiforov MP, Thompson GL, Reukov VV, Jesse S, Guo S, et al. 2010. Double-layer mediated electromechanical response of amyloid fibrils in liquid environment. *ACS Nano* 4:689–98
41. Jesse S, Baddorf AP, Kalinin SV. 2006. Switching spectroscopy piezoresponse force microscopy of ferroelectric materials. *Appl. Phys. Lett.* 88:062908
42. Rodriguez BJ, Jesse S, Alexe M, Kalinin SV. 2008. Spatially resolved mapping of polarization switching behavior in nanoscale ferroelectrics. *Adv. Mater.* 20:109–14
43. Jesse S, Rodriguez BJ, Choudhury S, Baddorf AP, Vrejoiu I, et al. 2008. Direct imaging of the spatial and energy distribution of nucleation centres in ferroelectric materials. *Nat. Mater.* 7:209–15
44. Tan Z, Roytburd AL, Levin I, Seal K, Rodriguez BJ, et al. 2008. Piezoelectric response of nanoscale $PbTiO_3$ in composite $PbTiO_3$–$CoFe_2O_4$ epitaxial films. *Appl. Phys. Lett.* 93:074101
45. Bintachitt P, Trolier-McKinstry S, Seal K, Jesse S, Kalinin SV. 2009. Switching spectroscopy piezoresponse force microscopy of polycrystalline capacitor structures. *Appl. Phys. Lett.* 94:042906
46. Seal K, Jesse S, Nikiforov MP, Kalinin SV, Fujii I, et al. 2009. Spatially resolved spectroscopic mapping of polarization reversal in polycrystalline ferroelectric films: crossing the resolution barrier. *Phys. Rev. Lett.* 103:057601
47. Wicks S, Seal K, Jesse S, Anbusathaiah V, Leach S, et al. 2010. Collective dynamics in nanostructured polycrystalline ferroelectric thin films using local time-resolved measurements and switching spectroscopy. *Acta Mater.* 58:67–75
48. Rodriguez BJ, Jesse S, Bokov AA, Ye ZG, Kalinin SV. 2009. Mapping bias-induced phase stability and random fields in relaxor ferroelectrics. *Appl. Phys. Lett.* 95:092904

49. Rodriguez BJ, Jesse S, Morozovska AN, Svechnikov SV, Kiselev DA, et al. 2010. Real space mapping of polarization dynamics and hysteresis loop formation in relaxor-ferroelectric $PbMg_{1/3}Nb_{2/3}O_3$-$PbTiO_3$ solid solutions. *J. Appl. Phys.* 108:042006
50. Rodriguez BJ, Jesse S, Kim J, Ducharme S, Kalinin SV. 2008. Local probing of relaxation time distributions in ferroelectric polymer nanomesas: time-resolved piezoresponse force spectroscopy and spectroscopic imaging. *Appl. Phys. Lett.* 92:232903
51. Kalinin SV, Rodriguez BJ, Jesse S, Morozovska AN, Bokov AA, Ye ZG. 2009. Spatial distribution of relaxation behavior on the surface of a ferroelectric relaxor in the ergodic phase. *Appl. Phys. Lett.* 95:142902
52. Kalinin SV, Rodriguez BJ, Budai JD, Jesse S, Morozovska AN, et al. 2010. Direct evidence of mesoscopic dynamic heterogeneities at the surfaces of ergodic ferroelectric relaxors. *Phys. Rev. B* 81:064107
53. Bintachitt P, Jesse S, Damjanovic D, Han Y, Reaney IM, et al. 2010. Collective dynamics underpins Rayleigh behavior in disordered polycrystalline ferroelectrics. *Proc. Natl. Acad. Sci. USA* 107:7219–24
54. Griggio F, Jesse S, Kumar A, Marincel DM, Tinberg DS, et al. 2011. Mapping piezoelectric nonlinearity in the Rayleigh regime using band excitation piezoresponse force microscopy. *Appl. Phys. Lett.* 98:212901
55. Jesse S, Maksymovych P, Kalinin SV. 2008. Rapid multidimensional data acquisition in scanning probe microscopy applied to local polarization dynamics and voltage dependent contact mechanics. *Appl. Phys. Lett.* 93:112903
56. Maksymovych P, Balke N, Jesse S, Huijben M, Ramesh R, et al. 2009. Defect-induced asymmetry of local hysteresis loops on $BiFeO_3$ surfaces. *J. Mater. Sci.* 44:5095–101
57. Balke N, Jesse S, Morozovska AN, Eliseev E, Chung DW, et al. 2010. Nanometer-scale electrochemical intercalation and diffusion mapping of Li-ion battery materials. *Nat. Nanotechnol.* 5:749–54
58. Anbusathaiah V, Jesse S, Arredondo MA, Kartawidjaja FC, Ovchinnikov OS, et al. 2010. Ferroelastic domain wall dynamics in ferroelectric bilayers. *Acta Mater.* 58:5316–25
59. McLachlan MA, McComb DW, Ryan MP, Morozovska AN, Eliseev EA, et al. 2011. Probing local and global ferroelectric phase stability and polarization switching in ordered macroporous PZT. *Adv. Funct. Mater.* 21:941–47
60. Kumar A, Ovchinnikov O, Guo S, Griggio F, Jesse S, et al. 2011. Spatially resolved mapping of disorder type and distribution in random systems using artificial neural network recognition. *Phys. Rev. B* 84:024203
61. Kim Y, Kumar A, Tselev A, Kravchenko II, Han H, et al. 2011. Non-linear phenomena in multiferroic nanocapacitors: joule heating and electromechanical effects. *ACS Nano* 22:9104–12
62. Nikiforov MP, Jesse S, Morozovska AN, Eliseev EA, Germinario LT, Kalinin SV. 2009. Probing the temperature dependence of the mechanical properties of polymers at the nanoscale with band excitation thermal scanning probe microscopy. *Nanotechnology* 20:395709
63. Nikiforov MP, Gam S, Jesse S, Composto RJ, Kalinin SV. 2010. Morphology mapping of phase-separated polymer films using nanothermal analysis. *Macromolecules* 43:6724–30
64. Nikiforov MP, Hohlbauch S, King WP, Voïtchovsky K, Contera SA, et al. 2011. Temperature-dependent phase transitions in zeptoliter volumes of a complex biological membrane. *Nanotechnology* 22:055709
65. Balke N, Jesse S, Kim Y, Adamczyk L, Tselev A, et al. 2010. Real space mapping of Li-ion transport in amorphous Si anodes with nanometer resolution. *Nano Lett.* 10:3420–25
66. Guo S, Jesse S, Kalnaus S, Balke N, Daniel C, Kalinin SV. 2011. Direct mapping of ion diffusion times on $LiCoO_2$ surfaces with nanometer resolution. *J. Electrochem. Soc.* 158:A982–90
67. Jesse S, Balke N, Eliseev E, Tselev A, Dudney N, et al. 2011. Direct mapping of ionic transport in a Si anode on the nanoscale: time-domain electrochemical strain spectroscopy. *ACS Nano* 5:9682–95
68. Ovchinnikov O, Jesse S, Guo S, Seal K, Bintachitt P, et al. 2010. Local measurements of Preisach density in polycrystalline ferroelectric capacitors using piezoresponse force spectroscopy. *Appl. Phys. Lett.* 96:112906
69. Guo S, Ovchinnikov OS, Curtis ME, Johnson MB, Jesse S, Kalinin SV. 2010. Spatially resolved probing of Preisach density in polycrystalline ferroelectric thin films. *J. Appl. Phys.* 108:084103
70. Balke N, Jesse S, Kim Y, Adamczyk L, Ivanov IN, et al. 2010. Decoupling electrochemical reaction and diffusion processes in ionically-conductive solids on the nanometer scale. *ACS Nano* 4:7349–57
71. Vasudevan R, Liu Y, Li J, Liang WI, Kumar A, et al. 2011. Nanoscale-control of phase variants in strain-engineered $BiFeO_3$. *Nano Lett.* 11:3346–54
72. Arruda TM, Kumar A, Kalinin SV, Jesse S. 2011. Mapping irreversible electrochemical processes on the nanoscale: ionic phenomena in Li ion conductive glass ceramics. *Nano Lett.* 11:4161–67

73. Kumar A, Ovchinnikov OS, Funakubo H, Jesse S, Kalinin SV. 2011. Real-space mapping of dynamic phenomena during hysteresis loop measurements: dynamic switching spectroscopy piezoresponse force microscopy. *Appl. Phys. Lett.* 98:202903
74. Kumar A, Ciucci F, Morozovska AN, Kalinin SV, Jesse S. 2011. Measuring oxygen reduction/evolution reactions on the nanoscale. *Nat. Chem.* 3:707–13
75. Yamanaka K, Ogiso H, Kolosov O. 1994. Analysis of subsurface imaging and effect of contact elasticity in the ultrasonic force microscope. *Jpn. J. Appl. Phys.* 33:3197–203
76. Rabe U, Arnold W. 1994. Acoustic microscopy by atomic force microscopy. *Appl. Phys. Lett.* 64:1493–95
77. Yamanaka K, Nakano S. 1998. Quantitative elasticity evaluation by contact resonance in an atomic force microscope. *Appl. Phys. A* 66:S313–17
78. Rabe U, Kester E, Arnold W. 1999. Probing linear and non-linear tip–sample interaction forces by atomic force acoustic microscopy. *Surf. Interface Anal.* 27:386–91
79. Rabe U, Amelio S, Kester E, Scherer V, Hirsekorn S, Arnold W. 2000. Quantitative determination of contact stiffness using atomic force acoustic microscopy. *Ultrasonics* 38:430–37
80. Yamanaka K, Maruyama Y, Tsuji T, Nakamoto K. 2001. Resonance frequency and Q factor mapping by ultrasonic atomic force microscopy. *Appl. Phys. Lett.* 78:1939–41
81. Kobayashi K, Yamada H, Matsushige K. 2002. Resonance tracking ultrasonic atomic force microscopy. *Surf. Interface Anal.* 33:89–91
82. Rabe U, Janser K, Arnold W. 1996. Vibrations of free and surface-coupled atomic force microscope cantilevers: theory and experiment. *Rev. Sci. Instrum.* 67:3281–93
83. Rabe U. 2006. Atomic force acoustic microscopy. In *Applied Scanning Probe Methods II*, ed. B Bhushan, H Fuchs, pp. 37–90. New York: Springer
84. Rabe U, Kopycinska M, Hirsekorn S, Saldana JM, Schneider G, Arnold W. 2002. High-resolution characterization of piezoelectric ceramics by ultrasonic scanning force microscopy techniques. *J. Phys. D* 35:2621–35
85. Kos A, Hurley D. 2008. Nanomechanical mapping with resonance tracking scanned probe microscope. *Meas. Sci. Technol.* 19:015504
86. Hurley D, Kopycinska-Müller M, Kos A, Geiss R. 2005. Nanoscale elastic-property measurements and mapping using atomic force acoustic microscopy methods. *Meas. Sci. Technol.* 16:2167–72
87. Stan G, King SW, Cook RF. 2012. Nanoscale mapping of contact stiffness and damping by contact resonance atomic force microscopy. *Nanotechnology* 23:215703
88. Killgore J, Yablon D, Tsou A, Gannepalli A, Yuya P, et al. 2011. Viscoelastic property mapping with contact resonance force microscopy. *Langmuir* 27:13983–87
89. Yablon DG, Gannepalli A, Proksch R, Killgore J, Hurley DC, et al. 2012. Quantitative viscoelastic mapping of polyolefin blends with contact resonance atomic force microscopy. *Macromolecules* 45:4363–70
90. van Heek KH. 2000. Progress of coal science in the 20th century. *Fuel* 79:1–26
91. Longwell JP, Rubin ES, Wilson J. 1995. Coal: energy for the future. *Prog. Energy Combust. Sci.* 21:269–360
92. Speight JG. 2012. *The Chemistry and Technology of Coal*. Boca Raton, FL: CRC. 3rd ed.
93. Son JY, Lee G, Shin YH. 2009. Surface charge dynamics on ferroelectric $PbZr_{0.48}Ti_{0.52}O_3$ films responding to the switching bias of electric force microscope. *Appl. Phys. Lett.* 94:162902
94. Pirc R, Blinc R, Bobnar V. 2001. Dynamics of relaxor ferroelectrics. *Phys. Rev. B* 63:054203
95. Balke N, Jesse S, Morozovska A, Eliseev E, Chung D, et al. 2010. Nanometer-scale electrochemical intercalation and diffusion mapping of Li-ion battery materials. *Nat. Nanotechnol.* 5:749–54
96. Kumar A, Ehara Y, Wada A, Funakubo H, Griggio F, et al. 2012. Dynamic piezoresponse force microscopy: spatially resolved probing of polarization dynamics in time and voltage domains. *J. Appl. Phys.* 112:052021
97. Haykin SO. 2008. *Neural Networks and Learning Machines*. Englewood Cliffs, NJ: Prentice Hall. 3rd ed.

Annual Review of
Physical Chemistry
Volume 65, 2014

Contents

Indexes

Errata

An online log of corrections to *Annual Review of Physical Chemistry* articles may be found at http://www.annualreviews.org/errata/physchem